Mar Biotechnol
DOI 10.1007/s10126-015-9642-z

SHORT COMMUNICATION

The Shark Strikes Twice: Hypervariable Loop 2 of Shark IgNAR Antibody Variable Domains and Its Potential to Function as an Autonomous Paratope

Stefan Zielonka[1] · Martin Empting[2] · Doreen Könning[1] · Julius Grzeschik[1] · Simon Krah[3] · Stefan Becker[3] · Stephan Dickgießer[1] · Harald Kolmar[1]

Received: 12 January 2015 / Accepted: 6 May 2015

Abstract In this present study, we engineered hypervariable loop 2 (HV2) of the IgNAR variable domain in a way that it solely facilitates antigen binding, potentially functioning as an autonomous paratope. For this, the surface-exposed loop corresponding to HV2 was diversified and antigen-specific variable domain of IgNAR antibody (vNAR) molecules were isolated by library screening using yeast surface display (YSD) as platform technology. An epithelial cell adhesion molecule (EpCAM)-specific vNAR was used as starting material, and nine residues in HV2 were randomized. Target-specific clones comprising a new HV2-mediated paratope were isolated against cluster of differentiation 3ε (CD3ε) and human Fcγ while retaining high affinity for EpCAM. Essentially, we demonstrate that a new paratope comprising moderate affinities against a given target molecule can be engineered into the vNAR scaffold that acts independent of the original antigen-binding site, composed of complementarity-determining region 3 (CDR3) and CDR1.

Keywords Antibody engineering · Antibody technology · Shark · IgNAR · Single-chain binding domain · Heavy chain antibody · Yeast surface display · Antigen-binding site

Introduction

Besides antibodies with the classical composition of heavy and light chains, sharks produce a heavy-chain only homodimer, referred to as IgNAR, in which antigen binding is mediated by a single variable domain, named variable domain of IgNAR antibody (vNAR) (Greenberg et al. 1995). Due to their high affinity and specificity in conjunction with their small size and high physicochemical stability, vNAR domains emerged as promising molecules for biomedical and biotechnological applications, and consequently, a plethora of antigen-specific vNAR molecules was isolated for various applications, as recently reviewed (Zielonka et al. 2014a). The vNAR domain displays several peculiar characteristics. By virtue of the deletion in the framework-2-complementarity-determining region (CDR) 2 region, vNAR is the smallest antibody-like antigen-binding domain in the animal kingdom known to date, with a molecular mass of approximately 12 kDa (Barelle et al. 2009; Stanfield et al. 2004). As a consequence, vNAR domains have only two complementary determining regions CDR1 and CDR3; the latter region primarily mediates antigen binding. After antigen contact, high rates of mutations cluster to the CDRs, to the CDR2 truncation site, where the remaining loop forms a belt-like structure at the bottom of the molecule and to a loop which corresponds to HV4 in T cell receptors (Fig. 1). Correspondingly, these mutation-prone regions have been named HV2 and HV4, respectively (Dooley et al. 2006; Zielonka et al. 2014a). vNAR domains can be categorized into four types, based on the presence and absence of non-

Electronic supplementary material The online version of this article (doi:10.1007/s10126-015-9642-z) contains supplementary material, which is available to authorized users.

✉ Harald Kolmar
Kolmar@Biochemie-TUD.de

[1] Institute for Organic Chemistry and Biochemistry, Technische Universität Darmstadt, Alarich-Weiss-Strasse 4, 64287 Darmstadt, Germany

[2] Helmholtz-Institute for Pharmaceutical Research Saarland (HIPS), Department Drug Design and Optimization, Saarland University, Campus C2.3, 66123 Saarbrücken, Germany

[3] Protein Engineering and Antibody Technologies, Merck-Serono, Merck KGaA, Frankfurter Straße 250, 64293 Darmstadt, Germany

Published online: 24 May 2015

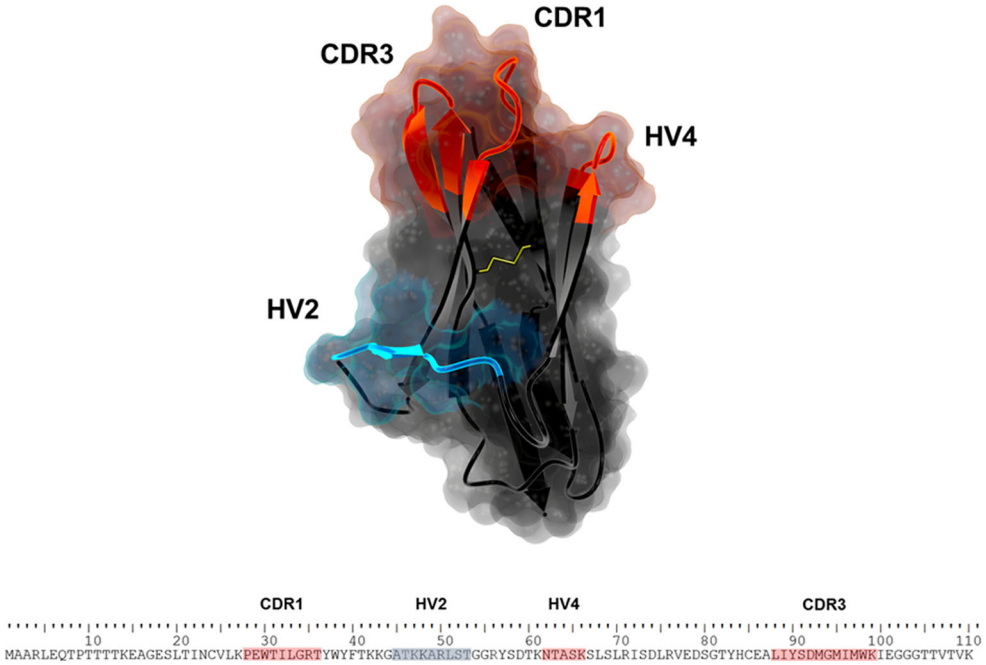

Fig. 1 Depiction of the rationale for the generation of a new antigen-binding site into the vNAR scaffold. The conventional paratope composed of CDR3 and CDR1 (and HV4) is shown in *red*. The potentially new antigen-binding site, consisting of HV2, is shown in *blue*. *Yellow*: disulfide bond. Model based on pdb entry 4HGK (Kovalenko et al. 2013) generated using YASARA structure (Krieger et al. 2009). Sequence shown for parental molecule 5005 used for library design. Sequence for CDR1 and CDR3 as well as HV4 of the conventional antigen-binding site shaded in *red*. Residues in sequence exposed loop corresponding to HV2 and considered for randomization shown in *blue*

canonical cysteine residues, which are not found in classical antibody variable domains (Diaz et al. 2002; Kovalenko et al. 2013; Stanfield et al. 2004; Stanfield et al. 2007; Streltsov et al. 2005; Zielonka et al. 2014a). Except for type I domains, HV2 is located distantly from the conventional antigen-binding site, composed of CDR3, CDR1, and HV4 (Fig. 1). However, for type I vNAR molecules, CDR3 is held tightly into the direction of HV2 (Stanfield et al. 2004). Consistent with this structural feature, mutations are favored in this loop for this particular type of domain, indicating that in this context, HV2 might participate in antigen binding (Flajnik et al. 2011; Stanfield et al. 2004).

Within this work, we set out to engineer HV2 in a type IV vNAR in a way that it solely facilitates antigen binding, independent from the conventional antigen-binding site composed of CDR3 and CDR1 (and HV4). For this, we randomized nine residues of HV2 of a high-affinity EpCAM-binding semisynthetic vNAR molecule, known as 5005 (Zielonka et al. 2014b). This particular molecule was isolated from a semisynthetic library where the regions corresponding to CDR1 and CDR3 were randomized. Hence, HV2 is not involved in antigen binding. Herein, we report the isolation of antigen-binding vNAR molecules with artificial HV2 loops against two different antigens, CD3ε and non-glycosylated human Fcγ, using yeast surface display. Interestingly, isolated binders retained high affinities against EpCAM, demonstrating that HV2 can potentially function as a paratope without compromising the structural and functional integrity of the vNAR scaffold. To the best of our knowledge, this approach for the generation of a new antigen-binding site has not been reported to date.

Materials and Methods

Media and Reagents

Yeast extract-peptone-dextrose (YPD) medium contained 20 g/L tryptone, 20 g/L dextrose, and 10 g/L yeast extract. Synthetic dextrose medium with casamino acids (SD-CAA) medium was composed of 1.7 g/L yeast nitrogen base without amino acids and ammonium sulfate, 5 g/L ammonium sulfate, 5 g/L Bacto casamino acids, 20 g/L dextrose, 8.6 g/L $NaH_2PO_4 \times H_2O$, and 5.4 g/L Na_2HPO_4. SG-CAA medium was prepared similarly except for the substitution of 20 g/L dextrose by galactose. Additionally, 10 % (*w*/*v*) polyethylene glycol 8000 (PEG 8000) was incorporated. Phosphate-buffered saline (PBS) contained 8.1 g/L NaCl, 0.75 g/L KCl, 1.13 g/L Na_2HPO_4, and 0.27 g/L KH_2PO_4, pH 7.4.

Recombinant human His-tagged EpCAM and recombinant human CD3ε were purchased from AcroBiosystems. Glycosylated human Fcγ was produced in-house. Non-glycosylated human Fcγ, produced in-house, carries an Asn297Ala mutation, preventing glycosylation.

Library Construction

pCT plasmid, carrying genetic information for EpCAM-specific vNAR molecule 5005 (Zielonka et al. 2014a), was used as template for HV2-randomized library construction. HV2 diversification was executed in a consecutive two-step splicing by overlap extension polymerase chain reaction (PCR) as depicted in Fig. 2a. For all reactions, the conditions were as follows: 94 °C for 2 min, 35 cycles of 30 s at 94 °C, 30 s at 55 °C, and 40 s at 72 °C, followed by 72 °C for 7 min. Primer sequences are listed in Table S1. For the first PCR step, two reactions were carried out in parallel, each containing isolated plasmid DNA as starting material. In one reaction, primer pair HV2_SOE_rand_up/pCT_Seq_lo was used. The forward primer randomized nine residues in the surface-exposed loop, corresponding to HV2. Residues considered for randomization are shown in Fig. 1. In the other reaction, primer pair pCT_Seq_up/HV2_SOE_lo was engaged. The respective PCR products were purified using Wizard® SV Gel and PCR Clean-up System (Promega) according to the manufacturer's instructions. For the subsequent PCR, 1 μL of each PCR product was used as template, respectively. After six cycles, primer pair pCT_Seq_up/pCT_Seq_lo was added. The resulting PCR product was purified via Wizard® SV Gel and PCR Clean-up System.

The pCT plasmid (Boder and Wittrup 1997), used for gap repair cloning and surface presentation of vNAR library candidates, was digested with *Nhe*I and *Bam*HI and purified via Wizard® SV Gel and PCR Clean-up System. For electroporation, 1–2 μg of the digested plasmid and 6–8 μg of insert were used. After 1-h incubation at 30 °C (1:1 YPD and 1 M sorbitol), library size was calculated by dilution plating. Yeast cells (EBY 100) were transferred into SD-CAA medium. Stocks were stored at −80 °C. For yeast surface display, cells were grown overnight at 30 °C in SD-CAA medium, transferred into SG-CAA medium, and incubated for 1–2 days at 20 °C.

Binding Assays on the Yeast Surface and Library Screening for the Isolation of Target-Specific vNAR Molecules

Procedures and protocols for yeast surface display of vNAR domains have already been described by our group (Zielonka et al. 2014b) and thus are herein only briefly described. Flow cytometry was used to analyze presentation on the yeast surface and for single-clone analysis. About 10^7 cells were

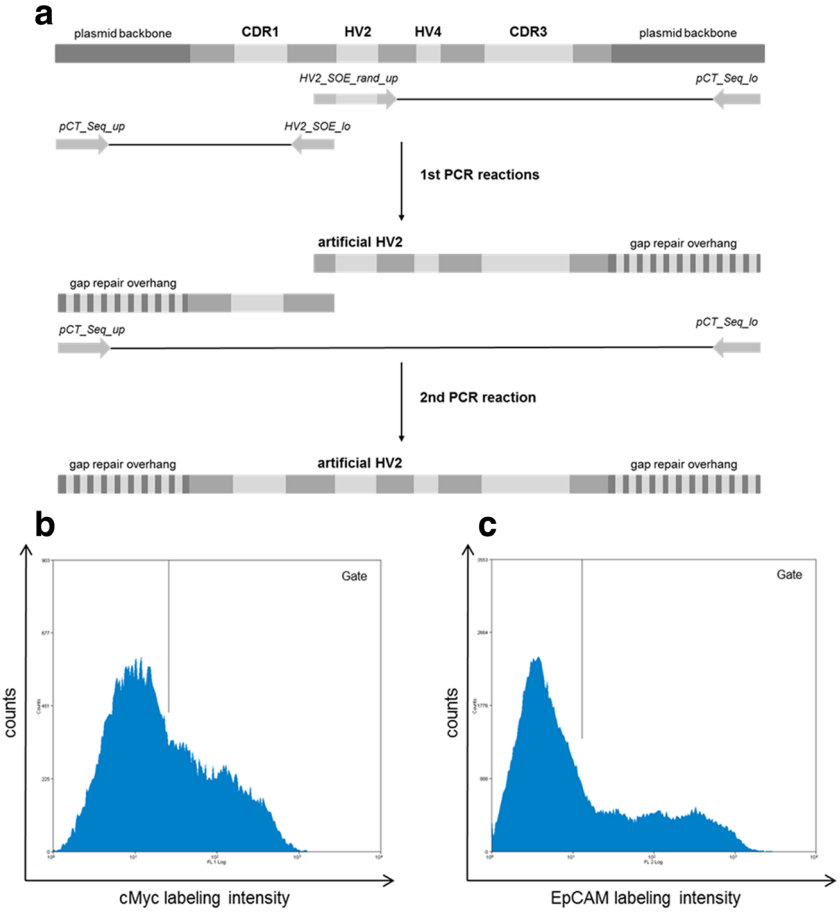

Fig. 2 **a** Schematic representation of PCR-based randomization of HV2. pCT plasmid encoding EpCAM-specific vNAR 5005 was used as template. In first PCRs, HV2 was randomized and the corresponding up and low fragments of the vNAR domain were constructed. In a subsequent reaction, the total vNAR molecule was constructed via splicing by overlap extension. **b**, **c** Analysis of HV2-randomized library based on EpCAM-specific vNAR 5005. Histogram of cMyc surface expression (**b**) and EpCAM binding (**c**) of the constructed vNAR library assessed by indirect immunofluorescence labeling and flow cytometry, 1 day postinduction. Cells in gate: 40.1 % for cMyc staining and 35.9 % for EpCAM labeling (1 μM EpCAM, detected with EpCAM-specific antibody clone HEA-125 conjugated to PE, Miltenyi Biotec)

labeled consecutively with anti-cMyc antibody (monoclonal, mouse, made in-house) and anti-mouse IgG FITC conjugate (goat, Sigma-Aldrich, diluted 1:10 in PBS) for at least 10 min on ice. For single-clone analysis, vNAR-presenting cells were either incubated with biotinylated, His-tagged CD3ε or Fcγ antigen for 15 min on ice, and subsequently stained with streptavidin-allophycocyanin (APC) (diluted 1:10), Penta-His Alexa Fluor 488 conjugate (Qiagen, diluted 1:30), or anti-Hu IgG (Fcγ-specific) PE (eBioscience, diluted 1:30) for 10 min. Plasmid DNA from positive clones was isolated and sent out for sequencing with pCT-seq_lo or pCT-seq_up oligonucleotide (Table S1).

Affinities of isolated vNAR variants on yeast cells were determined as described (Chao et al. 2006; Van Antwerp and Wittrup 2000; Zielonka et al. 2014b). Flow cytometric analysis was performed to determine antigen binding. At least eight different antigen concentrations were used, and cells were incubated for at least 1 h with the respective antigen. For the final calculation, RFU was plotted against antigen concentration.

Library screening for the isolation of antigen-specific vNAR molecules was performed on a MoFlo cell sorter (Beckman Coulter) and analyzed via Summit 4.3. For two-dimensional screening, cells were resuspended in PBS containing the desired concentrations of both antigens and incubated on ice for at least 30 min. Subsequently, antigen binding was detected using streptavidin-APC conjugate (diluted 1:10), Penta-His Alexa Fluor 488 conjugate, anti-Hu IgG (Fcγ-specific) PE, or Fcγ-specific Fab fragment conjugated to Alexa Fluor 488 (Jackson ImmunoResearch, diluted 1:30). For the first rounds of sorting of the initial library, approximately 2×10^8 cells were analyzed and sorted. Consecutive rounds were at least performed with a tenfold excess of cells that were collected in the previous round to ensure coverage of the enriched population.

Results and Discussion

The artificial HV2-randomized library for yeast surface display was constructed by polymerase chain reaction (PCR) using plasmid-encoded EpCAM-specific clone 5005 as starting material. In the framework of this clone, nine residues in HV2 were totally diversified by the incorporation of trinucleotide mixtures encoding all 19 amino acids except cysteine into the corresponding oligonucleotide. Residues considered for library design are given in Fig. 1 (blue residues). The library was established in a consecutive two-step splicing by overlap extension PCR, as depicted in Fig. 2a, and a yeast surface display library with an estimated diversity of approximately 1×10^9 unique clones (calculated by dilution plating) was constructed in a homologous recombination-based process referred to as plasmid gap repair (Benatuil et al. 2010). As already described (Zielonka et al. 2014b), library-encoded HV2-randomized vNAR fragments were displayed on the yeast surface via Aga1p/Aga2p association (Boder and Wittrup 1997). vNARs were expressed as fusion protein with HA-tag and cMyc epitope at the *N*-terminus and *C*-terminus, respectively, for the detection of surface-displayed library candidates. Surface presentation as well as maintenance of structural integrity, i.e., EpCAM binding of HV2-randomized library candidates, was assessed by indirect fluorescence labeling of the cMyc epitope or via EpCAM binding assays on the yeast surface (Fig. 2b, c). Within 1 day postinduction, there was more than 40 % cMyc-tag expression of the library detectable and about 36 % of EpCAM labeling, indicating that the vast majority of displayed vNAR fragments retained their structural integrity after randomization of HV2. These findings are consistent with the observation that HV2 is a mutation-prone region (Dooley et al. 2006; Flajnik et al. 2011; Stanfield et al. 2004), potentially tolerating a high degree of diversity at the sequence level as well as structural multiplicity.

To evaluate whether this loop can potentially function as a distinct antigen-binding site, the library was screened against two different targets, CD3ε and non-glycosylated human Fcγ. To isolate binders, targeting a new antigen with HV2 while retaining affinity against EpCAM, first and last rounds of screening were performed two dimensionally for target binding (Fig. 3). To this end, vNAR binding of His-tagged EpCAM was detected using an Alexa Fluor 488-labeled anti-His-tag antibody. Binding to CD3ε was detected using biotinylated antigen as well as streptavidin-APC. To avoid off-target binding against detection reagents, the labeling strategy was alternated from using biotinylated CD3ε to His-tagged antigen which was detected via Alexa Fluor 488-labeled anti-His-tag antibody. Consequently, we only sorted for CD3ε binding. Initial FACS sorting rounds were performed with 1 μM EpCAM and 2 μM CD3ε. To enhance screening stringency and, hence, to obtain binders against CD3ε displaying adequate affinities, the respective target protein concentration was reduced to 1 μM in rounds 3 and 4. As shown in Fig. 3, we were able to enrich cells displaying a double-positive antigen-specific signal for EpCAM and CD3ε within four rounds of FACS sorting. Interestingly, we also enriched for a population which lost its ability for EpCAM binding, indicating that this particular population lost its structural integrity (Fig. 3).

Likewise, sorting carried out against non-glycosylated human Fcγ protein also revealed a significant enrichment of FACS double-positive clones (Fig. S1). In these particular screening experiments, binding to human Fcγ was detected using either anti-human Fcγ-specific IgG conjugated to PE (rounds 1, 3, and 4) or Fcγ-specific Fab fragment conjugated to Alexa Fluor 488 (sorting round 2).

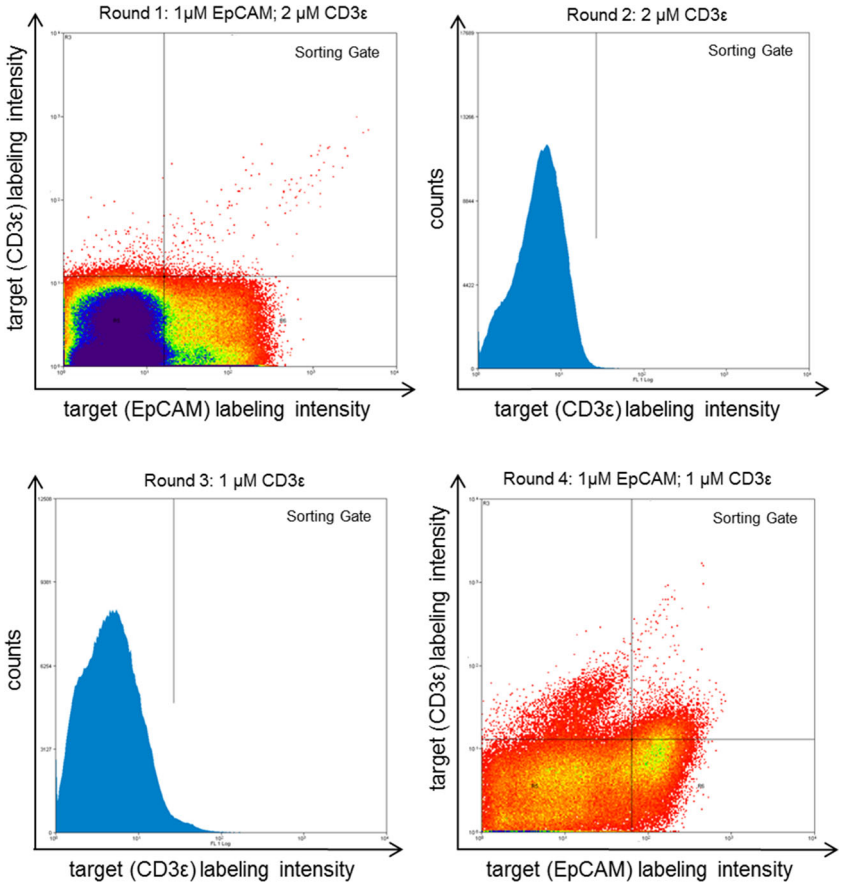

Fig. 3 Screening of a HV2-randomized EpCAM-specific library based on vNAR 5005 against CD3ε. Sorting gates and target concentrations are shown. In rounds 1 and 4, cells were simultaneously labeled for EpCAM binding using Penta-His Alexa Fluor 488 conjugate and CD3ε binding via biotinylated antigen and streptavidin-APC. In rounds 2 and 3, cells were only labeled for CD3ε binding using His-tagged antigen and Penta-His Alexa Fluor 488 conjugate. After round 3, a resort was performed. Cells in the sorting gate were isolated, grown, and induced for the next round of selection. Target-positive cells in sorting gate: (R1) 0.1 %, (R2) 0.17 %, (R3) 1.92 %, and (R4) 5.8 %

Single clones were analyzed in terms of their ability to target both antigens, EpCAM and CD3ε, and double-positive clones were sent out for sequencing, resulting in the identification of several double-positive clones (Fig. S2). Importantly, all identified clones were direct progenies of parental molecule 5005, each comprising a unique sequence in HV2, resulting from library design. Most of the clones still bound strongly to EpCAM at a concentration of 1 μM, but binding to CD3ε was very weak at 1 μM, as exemplarily shown for single-clone H5 (Fig. S3). Notwithstanding, for one clone, referred to as clone B1, we observed binding to CD3ε to a significantly higher extent compared to all other analyzed clones, whereas for parental molecule 5005, no binding was observed against CD3ε at the highest concentration tested (Fig. 4). Since it was evidenced that yeast surface display allows for the instantaneous characterization of isolated

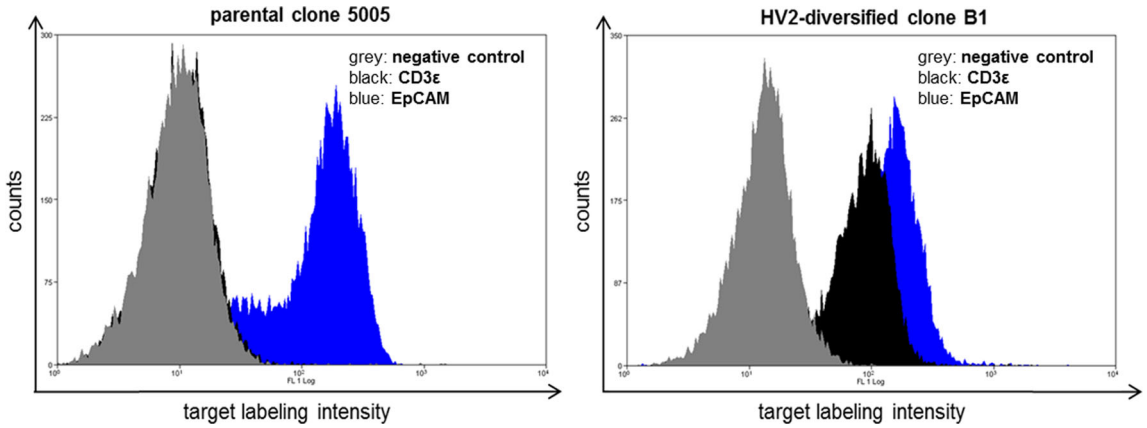

Fig. 4 Single-clone analysis of monospecific, parental clone 5005 and HV2-diversified clone B1 for EpCAM and CD3ε binding. Single clones were incubated with 1 μM of the respective antigen. Alexa Fluor 488-labeled anti-His-tag antibody was used for the detection of target binding. *Blue*: cells stained with EpCAM. *Black*: cells incubated with CD3ε. *Gray*: negative control, cells only labeled with secondary detection antibody

Table 1 Equilibrium dissociation constants (K_D) determined by yeast surface display for HV-diversified clones compared to parental clone 5005

vNAR clone	Type of molecule	K_D (nM) EpCAM	K_D (nM) CD3ε/Fcγ
5005	Parental molecule	40±13	– (CD3ε/Fcγ)
B1	After library screen CD3ε	46±8	422±60 (CD3ε)
F1	After library screen human Fcγ	53±10	~2600 (Fcγ)

binders in terms of affinity and stability without the need for soluble expression (Doerner et al. 2014; Gai and Wittrup 2007; Van Antwerp and Wittrup 2000; Zielonka et al. 2014b), we decided to determine equilibrium binding constants via affinity titration on cells, as given in Table 1. Binder B1 displayed affinities for CD3ε of about 400 nM, without significantly compromising the affinity against EpCAM, compared to its parental molecule 5005. Importantly, selectivity assays conducted on the yeast surface revealed that no non-specific binding was observable against unrelated target proteins (Fig. S4).

Akin to these observations, one double-positive EpCAM- and human Fcγ-binding clone, referred to as clone F1, was identified after single-clone analysis (Fig. S2). Characterization of this clone resulted in a moderate affinity against human Fcγ of approximately 2.6 μM. Furthermore, no significant off-target binding was detected against unrelated target proteins (Fig. S4). Affinity against EpCAM was comparable to that of its parental clone 5005, which does not display detectable binding to human Fcγ, as listed in Table 1. In this respect, no efforts were made to optimize affinities against Fcγ via alanine scanning and sub-library screening. Interestingly, this clone only bound to non-glycosylated human Fcγ. For the glycosylated equivalent, we were unable to detect any binding at the highest concentrations tested (Fig. 5). Hence, one can draw conclusions with regard to the epitope that is addressed by clone F1. It is tempting to speculate that position 297 of Fcγ is involved in the vNAR-target interaction, since for wild-type Fcγ, this residue is Asn which is typically glycosylated. However, unglycosylated Fcγ contains an Asn to Ala mutation at this position, and it can be assumed that this mutation, which prevents glycosylation, is part of the epitope targeted by HV2-diversified clone F1. Another hypothesis is that glycosylation of the Fc fragment covers the epitope targeted by α-EpCAM-Fcγ-vNAR F1 in a way that this region as structurally not accessible.

The immunoglobulin family displays a paramount tolerability in loop length as well as sequence variation, which is most evident for CDR regions of variable domains. However, this feature is a general hallmark of the immunoglobulin domains (Halaby et al. 1999; Wozniak-Knopp et al. 2010) and loop regions other than the natural CDRs can be considered for engineering novel binding characteristics. In this respect, surface-exposed loops at the *N*-terminal tip of CH2 of human IgG have been engineered for antigen binding (Xiao et al. 2009). In another very elegant approach, established by Rüker and co-workers, a new antigen-binding site was introduced in loop regions of the CH3 domain of human IgG (Wozniak-Knopp et al. 2010). Most importantly, those engineered Fc fragments, named Fcab, retained the ability to elicit effector functions, clearly indicating the structural integrity of the molecule.

Essentially, our study demonstrates that the vNAR scaffold can be engineered in a way that HV2 potentially functions as an independent paratope, exclusively facilitating antigen binding against a target protein. Importantly, the establishment of a new binding functionality does not impair the conventional antigen-binding site, composed of CDR3 and CDR1 in its

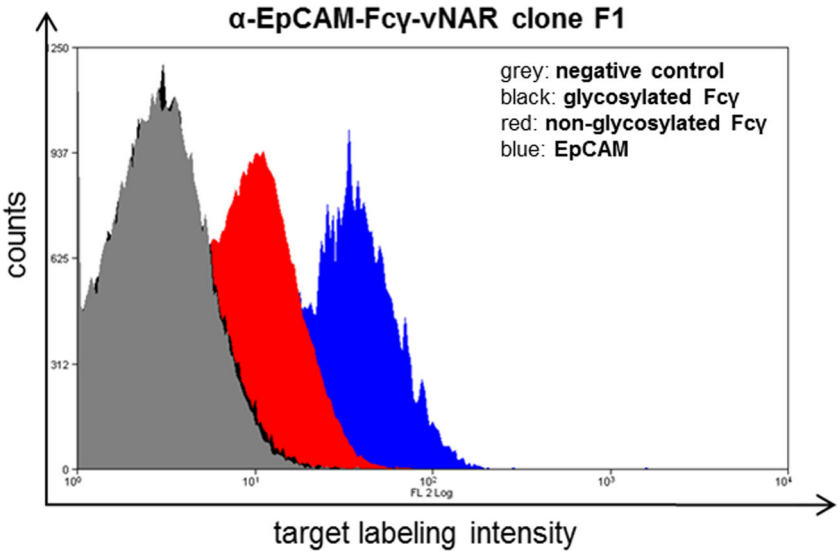

Fig. 5 Single-clone analysis of EpCAM- and non-glycosylated Fcγ-binding HV2-diversified clone F1. Single clone was incubated with 1 μM of the respective antigen. Anti-human IgG conjugated to PE (Fcγ-specific) was used for the detection of target binding. *Gray*: negative control, cells only labeled with secondary detection antibody. *Black*: cells incubated with glycosylated Fcγ. *Red*: cells labeled with non-glycosylated Fcγ. *Blue*: cells labeled with EpCAM and detected via EpCAM-specific antibody clone HEA-125 conjugated to PE (Miltenyi Biotec)

affinity. However, it needs to be mentioned that affinities mediated by HV2 are only moderate and almost certainly require optimization for further studies such as effector cell recruitment assays. In this respect, affinity maturation might be performed by second-generation randomization of the HV2-adjacent surface-exposed loop, referred to as EF-loop, as already described by Wozniak-Knopp et al. for human constant CH3 domains (Wozniak-Knopp et al. 2010). This group utilized the EF-loop in CH3 as part of a novel antigen-binding site.

In recent years, bispecific antibodies and antibody domains have opened new avenues for the treatment of various diseases (Kontermann 2012; Weidle et al. 2014). Ultimately, it remains to be elucidated whether shark-derived antibody domains may contribute to this continuously evolving field of therapeutic drug design in the future.

Acknowledgments This work was supported in part by the Federal Ministry of Education and Research (BMBF) in frame of the consortium Nanokat. We thank Prof. Dr. Siegfried Neumann for general advice.

Conflict of Interest The authors declare no potential conflicts of interest.

References

Barelle C, Gill DS, Charlton K (2009) Shark novel antigen receptors—the next generation of biologic therapeutics? Adv Exp Med Biol 655: 49–62. doi:10.1007/978-1-4419-1132-2_6

Benatuil L, Perez JM, Belk J, Hsieh CM (2010) An improved yeast transformation method for the generation of very large human antibody libraries. Protein Eng Des Sel 23:155–159. doi:10.1093/protein/gzq002

Boder ET, Wittrup KD (1997) Yeast surface display for screening combinatorial polypeptide libraries. Nat Biotechnol 15:553–557. doi:10.1038/nbt0697-553

Chao G, Lau WL, Hackel BJ, Sazinsky SL, Lippow SM, Wittrup KD (2006) Isolating and engineering human antibodies using yeast surface display. Nat Protoc 1:755–768. doi:10.1038/nprot.2006.94

Diaz M, Stanfield RL, Greenberg AS, Flajnik MF (2002) Structural analysis, selection, and ontogeny of the shark new antigen receptor (IgNAR): identification of a new locus preferentially expressed in early development. Immunogenetics 54:501–512. doi:10.1007/s00251-002-0479-z

Doerner A, Rhiel L, Zielonka S, Kolmar H (2014) Therapeutic antibody engineering by high efficiency cell screening. FEBS Lett 588:278–287. doi:10.1016/j.febslet.2013.11.025

Dooley H, Stanfield RL, Brady RA, Flajnik MF (2006) First molecular and biochemical analysis of in vivo affinity maturation in an ectothermic vertebrate. Proc Natl Acad Sci U S A 103:1846–1851. doi:10.1073/pnas.0508341103

Flajnik MF, Deschacht N, Muyldermans S (2011) A case of convergence: why did a simple alternative to canonical antibodies arise in sharks and camels? PLoS Bio l9:e1001120. doi:10.1371/journal.pbio.1001120

Gai SA, Wittrup KD (2007) Yeast surface display for protein engineering and characterization. Curr Opin Struct Biol 17:467–473. doi:10.1016/j.sbi.2007.08.012

Greenberg AS, Avila D, Hughes M, Hughes A, McKinney EC, Flajnik MF (1995) A new antigen receptor gene family that undergoes rearrangement and extensive somatic diversification in sharks. Nature 374:168–173. doi:10.1038/374168a0

Halaby DM, Poupon A, Mornon J (1999) The immunoglobulin fold family: sequence analysis and 3D structure comparisons. Protein Eng 12:563–571

Kontermann RE (2012) Dual targeting strategies with bispecific antibodies. mAbs 4:182–197. doi:10.4161/mabs.4.2.19000

Kovalenko OV et al (2013) Atypical antigen recognition mode of a shark immunoglobulin new antigen receptor (IgNAR) variable domain characterized by humanization and structural analysis. J Biol Chem 288:17408–17419. doi:10.1074/jbc.M112.435289

Krieger E et al (2009) Improving physical realism, stereochemistry, and side-chain accuracy in homology modeling: four approaches that performed well in CASP8. Proteins 77(Suppl 9):114–122. doi:10.1002/prot.22570

Stanfield RL, Dooley H, Flajnik MF, Wilson IA (2004) Crystal structure of a shark single-domain antibody V region in complex with lysozyme. Science 305:1770–1773. doi:10.1126/science.1101148

Stanfield RL, Dooley H, Verdino P, Flajnik MF, Wilson IA (2007) Maturation of shark single-domain (IgNAR) antibodies: evidence for induced-fit binding. J Mol Biol 367:358–372. doi:10.1016/j.jmb.2006.12.045

Streltsov VA, Carmichael JA, Nuttall SD (2005) Structure of a shark IgNAR antibody variable domain and modeling of an early-developmental isotype. Protein Sci 14:2901–2909. doi:10.1110/ps.051709505

Van Antwerp JJ, Wittrup KD (2000) Fine affinity discrimination by yeast surface display and flow cytometry. Biotechnol Prog 16:31–37. doi:10.1021/bp990133s

Weidle UH, Kontermann RE, Brinkmann U (2014) Tumor-antigen-binding bispecific antibodies for cancer treatment. Semin Oncol 41:653–660. doi:10.1053/j.seminoncol.2014.08.004

Wozniak-Knopp G et al (2010) Introducing antigen-binding sites in structural loops of immunoglobulin constant domains: Fc fragments with engineered HER2/neu-binding sites and antibody properties. Proc Natl Acad Sci U S A 23:289–297. doi:10.1093/protein/gzq005

Xiao X, Feng Y, Vu BK, Ishima R, Dimitrov DS (2009) A large library based on a novel (CH2) scaffold: identification of HIV-1 inhibitors. Biochem Biophys Res Commun 387:387–392. doi:10.1016/j.bbrc.2009.07.044

Zielonka S, Empting M, Grzeschik J, Konning D, Barelle CJ, Kolmar H (2014a) Structural insights and biomedical potential of IgNAR scaffolds from sharks. mAbs. doi:10.4161/19420862.2015.989032

Zielonka S et al (2014b) Shark attack: high affinity binding proteins derived from shark vNAR domains by stepwise in vitro affinity maturation. J Biotechnol 191:236–245. doi:10.1016/j.jbiotec.2014.04.023